Journal for ImmunoTherapy of Cancer

Blocking LIF and PD-L1 enhances the antitumor efficacy of SBRT in murine PDAC models

Jian Ye ,[1,2] Shuyang S Qin,[1,3] Angela L Hughson,[1,2] Gary Hannon ,[1,2] Noah A Salama,[3] Tara G Vrooman,[1,2,3] Maggie L Lesch,[1,2,3] Sidney Lesser,[1,2] Sarah L Eckl,[1,2,3] Rachel Jewell,[1,2] Lauren Benoodt,[4] Bradley N Mills,[1,2,5] Carl J Johnston,[5,6] Edith Lord,[2,3] Brian A Belt,[1,2] Laura M Calvi,[5,7] David Linehan,[1,2,5] Nadia Luheshi,[8] Jim Eyles,[9] Scott A Gerber[1,2,3,5]

To cite: Ye J, Qin SS, Hughson AL, *et al*. Blocking LIF and PD-L1 enhances the antitumor efficacy of SBRT in murine PDAC models. *Journal for ImmunoTherapy of Cancer* 2025;**13**:e010820. doi:10.1136/jitc-2024-010820

► Additional supplemental material is published online only. To view, please visit the journal online (https://doi.org/10.1136/jitc-2024-010820).

Accepted 21 April 2025

For numbered affiliations see end of article.

Correspondence to
Dr Scott A Gerber;
scott_gerber@urmc.rochester.edu

ABSTRACT

Background Recent preclinical and clinical data suggest that leukemia inhibitory factor (LIF) is a potential target for various tumor types including pancreatic ductal adenocarcinoma as LIF is involved in multiple protumor processes including cancer stem cell maintenance, epithelial–mesenchymal transition (EMT), immunosuppression, and chemo/radioresistance. Anti-LIF antibody therapy has demonstrated safety and tolerability but limited efficacy in phase 1 clinical trial in advanced solid tumors. This prompted us to explore combination therapies, suggesting that LIF blockade, when combined with standard-of-care chemotherapy, radiotherapy, and/or immunotherapy, could present a promising therapeutic strategy.

Methods We evaluated the impact of combining systemic inhibition of LIF/programmed death-ligand 1 (PD-L1) with localized stereotactic body radiotherapy (SBRT) on tumor progression across multiple murine orthotopic pancreatic tumor models and examined systemic antitumor immunity using a hepatic rechallenge model. The antitumor immune response was characterized throughflow cytometry and Luminex assays. To identify differentially expressed genes and signaling pathways following treatment, we performed bulk RNA sequencing on pancreatic tumors. Additionally, single-cell RNA sequencing was conducted to further examine changes in tumor-infiltrating immune cells and their signaling pathways.

Results We showed that simultaneous inhibition of LIF and PD-L1 significantly amplified the antitumor efficacy of SBRT, resulting in extended survival. The triple therapy (SBRT+anti-LIF+anti-PD-L1) generated an immunostimulatory tumor microenvironment, characterized by a proinflammatory shift in the cytokine/chemokine profile, increased infiltration of effector $CD8^+$ T cells, and upregulated activation or maturation signals in tumor-infiltrating $CD8^+$ T cells and macrophages. The beneficial effects of triple therapy were mostly abrogated by depletion of $CD8^+$ T cells. In addition, triple therapy downregulated pathways related to tumor stemness, proliferation, and metabolism, and reduced EMT. Importantly, the combination of local SBRT treatment with systemic LIF and PD-L1 blockade resulted in long-term systemic antitumor memory.

WHAT IS ALREADY KNOWN ON THIS TOPIC

⇒ Emerging evidence suggests that leukemia inhibitory factor (LIF) is a promising biomarker and target for pancreatic ductal adenocarcinoma (PDAC). A phase 1 clinical trial with anti-LIF antibody demonstrated safety but limited efficacy. It remains to be determined whether blockade of both LIF and programmed death-ligand 1 (PD-L1), along with stereotactic body radiotherapy (SBRT) enhances antitumor efficacy in both local and metastatic PDAC models.

WHAT THIS STUDY ADDS

⇒ Blockade of both LIF and PD-L1 significantly enhanced the antitumor effects of local SBRT in orthotopic PDAC murine models by shifting the immunosuppressive tumor microenvironment toward a more immunostimulatory phenotype that included a proinflammatory cytokine/chemokine profile, increased infiltration of effector $CD8^+$ T cells, and enhanced activation and maturation of tumor-infiltrating $CD8^+$ T cells and macrophages. The efficacy of triple therapy was primarily dependent on $CD8^+$ T cells. Notably, local SBRT combined with systemic blockade of LIF and PD-L1 induced long-term systemic antitumor memory.

HOW THIS STUDY MIGHT AFFECT RESEARCH, PRACTICE OR POLICY

⇒ The combination of SBRT with LIF and PD-L1 blockade has the potential to generate both local and long-lasting systemic antitumor immune responses in PDAC. This work provides a proof of concept for advancing this triple therapy regimen into clinical studies for human PDAC.

BACKGROUND

Pancreatic ductal adenocarcinoma (PDAC) is predicted to become the second deadliest cancer by 2030, presently holding the fourth position among cancer-related fatalities in the USA.[1 2] While showing promising benefits across various tumor types, immune checkpoint blockade (ICB) has proven ineffective

for PDAC, largely due to the unique immunosuppressive tumor microenvironment (TME) of PDAC.[3–7] Hence, the current challenge is to surmount the barrier of the immunosuppressive TME and transition it into an immunostimulatory environment. Our previous studies have indicated that radiotherapy, such as stereotactic body radiotherapy (SBRT), is a suitable candidate for combination with ICB due to its immunomodulatory effects, in contrast to chemotherapy. However, additional interventions are still necessary to reverse the immunosuppressive PDAC.[8 9]

Leukemia inhibitory factor (LIF) is a multifunctional cytokine and a member of the interleukin (IL)-6 family, which also includes IL-6, IL-11, IL-27, ciliary neurotrophic factor, cardiotrophin 1, cardiotrophin-like cytokine, and oncostatin M. LIF forms a ternary complex (1:1:1) with glycoprotein 130 (gp130) and the LIF receptor (LIFR) on the cell surface. The intracellular chains of LIFR and gp130 bind to Janus kinase 1 (JAK1), triggering downstream pathways such as JAK/STAT3, MAPK, PI(3)K, YAP, and mTOR signaling. These pathways regulate diverse cellular processes including self-renewal, differentiation, and survival.[10 11] Originally identified for its role in inducing the differentiation of leukemia cells, LIF has emerged as a key regulator in tumor-promoting processes in various cancers by regulating the self-renewal of cancer stem cells,[12–14] activating cancer-associated fibroblasts,[15] and promoting suppressive myeloid cells.[16] Additionally, LIF facilitates tumor cell proliferation[14 17] and confers resistance to chemotherapy[14] and radiotherapy.[18] Clinically, high expression of LIF is associated with poor prognosis and resistance to anticancer therapies.[12 15 18] Notably, recent clinical and preclinical studies highlight serum LIF as a promising diagnostic, prognostic, and disease progression biomarker for PDAC, demonstrating superior sensitivity and specificity compared with traditional markers, such as Carbohydrate Antigen 19-9 (CA19-9) and Carcinoembryonic Antigen (CEA).[14] However, while these findings are encouraging, the potential role of LIF as a biomarker, as well as the mechanistic involvement of LIF in areas such as immunosuppression and radioresistance, is not necessarily exclusive to PDAC, as LIF has also been implicated in other cancer types. Further confirmation in larger clinical studies is required to better define the specificity and utility of LIF across cancers.

Given its potential to influence multiple cancer mechanisms, inhibiting LIF represents a promising novel therapeutic strategy. Neutralizing antibodies and small-molecular inhibitors targeting the LIF/LIFR axis have been developed for preclinical studies or clinical evaluation.[15 19–23] Notably, MSC-1 (AZD0171), a humanized monoclonal antibody, has shown potent and specific LIF blockade across multiple cancer types.[24] Although the phase 1 trial of MSC-1 confirmed safety and tolerability as a monotherapy, the modest efficacy observed[25] suggests that inhibition of LIF may require combination with standard-of-care therapies, such as chemotherapy, radiotherapy, or immunotherapy, to achieve optimal therapeutic outcomes.

In this study, we evaluated the therapeutic potential of combining SBRT, anti-LIF, and anti-programmed death-ligand 1 (PD-L1) in preclinical PDAC models. The triple therapy (SBRT+anti LIF + anti-PD-L1) achieved significantly improved local tumor control and prolonged survival compared with untreated controls or monotherapy/dual therapy across multiple orthotopic PDAC mouse models. The triple therapy regimen fostered an immunostimulatory TME, marked by proinflammatory cytokine/chemokine profiles, increased infiltration of effector $CD8^+$ T cells, and enhanced activation/maturation signaling in both tumor-infiltrating $CD8^+$ T cells and macrophages. The therapeutic efficacy was primarily dependent on $CD8^+$ T cells, as their depletion nearly abolished the antitumor effect. Additionally, the triple therapy suppressed tumor stemness, proliferation, metabolic signaling, and epithelial–mesenchymal transition (EMT). Importantly, the integration of local SBRT with systemic LIF and PD-L1 blockade generated durable systemic antitumor memory. Together, these preclinical findings demonstrate that combining SBRT with LIF and PD-L1 inhibition represents a promising multimodal approach for PDAC treatment.

METHODS

Cells and reagents

The murine PDAC KCKO and luciferase-expressing KCKO (KCKO-Luc) cell lines were kindly provided by Dr Pinku Mukherjee (University of North Carolina, Charlotte, North Carolina, USA). KP2.1-Luc was generated by transfecting KP2 cells (obtained from Dr David DeNardo, Washington University of Medicine, St Louis, Missouri, USA) with luciferase-containing vectors (#LVP571-PBS, GenTarget). All cell lines were maintained in RPMI1640 supplemented with 10% fetal bovine serum (FBS) and 1% penicillin-streptomycin, regularly tested for *Mycoplasma* contamination, and used within three passages to ensure experimental consistency.

Anti-LIF (mAZD0171), anti-PD-L1 (Clone 80) and corresponding isotype IgG controls were provided by AstraZeneca. For in vivo studies, antibodies were administered intraperitoneally (20 mg/kg, 10 mg/kg anti-PD-L1 or matched isotype IgG control in 100 µl phosphate-buffered saline (PBS)) two times per week, starting 1 day before SBRT. For T cell depletion, mice received 200 µg of anti-CD4 (clone: YTS191), anti-CD8 (clone: 53–6.7), or isotype IgG (diluted in 100 µl PBS) every 3 days via intraperitoneal injection.

Murine orthotopic model and hepatic metastases model of pancreatic cancer

Female C57BL/6J mice (6–8 weeks old; Jackson Laboratory) were acclimated in our facility prior to experiments with all procedures approved by the University Committee on Animal Resources (UCAR) at the University of Rochester Medical Center (Rochester, New York, USA). We established orthotopic and hepatic metastasis

models with minor modifications from published protocols.[8 26 27] For the orthotopic implantation, anesthetized mice received 2×10^5 KCKO-Luc cells or 5×10^4 KP2.1-Luc cells suspended in a 1:1 mixture of PBS and Matrigel via the pancreatic tail injection, with titanium clips placed to mark the tumor for SBRT. In the rechallenge model, mice cured of primary tumors by triple therapy (SBRT+anti-LIF + anti-PD-L1) received 5×10^5 KCKO-Luc or KP2-Luc cells via hemispleen to induce hepatic metastases.

SBRT treatment

As previously described,[8 26–28] mice were anesthetized with isoflurane for x-irradiation using a Small Animal Radiation Research Platform (XStrahl SARRP: X-rays 220 kVp 13.0 mA at a dose rate of 3.1 Gy/min). The SARRP is equipped with CT-image guidance for target delineation and uses collimated radiation beams to cover only the defined target volume. Treatment planning was accomplished using the on-board MuriPlan software to identify the target and deliver the prescribed dose. The location of each pancreatic tumor was defined using two small titanium fiducial clips placed on either side of the tumor at the time of tumor injection. The clips were localized using CT imaging and used to precisely target two parallel opposing 5 mm × 5 mm collimated beams to the tumor volume while minimizing radiation exposure to surrounding normal tissues. A dose of 6 Gy was delivered to the tumor for four consecutive days (day 7–10 post-tumor inoculation). Radiographic film dosimetry was conducted prior to the experiment for treatment verification and quality assurance of radiation dose and dose distribution. Radiation-related side effects, such as weight loss or diarrhea, were not observed in this model (data not shown), likely due to the precise targeting of SBRT.

Flow cytometry

Tumor samples were processed into single-cell suspension using enzymatic digestion (30% collagenase, 37°C, 30 min) and mechanical dissociation, followed by filtration through 40 µm strainer.[8 27] Cells were suspended in PBS with 5% FBS and pretreated with Fc receptor blocking solution to minimize non-specific binding. For surface marker staining, cells were stained in the dark at 4° C for 30 min using the following fluorophore-conjugated antibodies (BD Biosciences or BioLegend): anti-CD45 (Fluorescein Isothiocyanate (FITC) or PE-Cy5), anti-CD3 (FITC), anti-CD4 (APC-Cy5), anti-CD8 (BV605), anti-NK1.1 (PE-Cy7), anti-CD11b (eFluor450), F4/80 (APC), anti-Ly6C (APC-Cy7), anti-Ly6G (PE-Cy7), anti-CD11c (PE-Cy7), anti-MHCII (PerCP-Cy5.5), anti-CD69 (APC), anti-PD-L1 (BV605), CD24 (BV605), anti-CD103 (APC), anti-XCR1 (BV421), anti-CD80 (BV786), anti-CD86 (BV510), anti-PD1 (BV711), and anti-CTLA4 (APC-R700). For intracellular staining, fixed and permeabilized cells (FoxP3/Transcription factor staining buffer set, eBiosciences) were stained with fluorescence-labeled antibodies including anti-IFNg (BV786) and anti-FoxP3 (APC) in the dark for 30 min at room temperature. Cells were analyzed on an LSR II Flow Cytometer (FlowJo V.10.10.0 for data analysis).

Immunohistochemical staining

Cleaved caspase-3, HMGB1, and HSP70-positive cells were evaluated by immunohistochemical staining, as detailed in prior studies.[8 26 27] Briefly, frozen tumor sections (KP2-Luc or KCKO-Luc tumors) were incubated overnight at 4°C with primary antibodies: anti-cleaved caspase-3 (#9664S, Cell Signaling), anti-HMGB1 (ab18256, Abcam), or anti-HSP70 (ab79852, Abcam), followed by rabbit antibody enhancer and Polymer horseradish peroxidase (#D39-18, GBI Labs). The tissues were developed with chromogen substrate, and counterstained with hematoxylin. Expression levels of these markers were quantified using the Aperio Image Scope algorithm (Leica Biosystems).

Analysis of cytokines and chemokines using multiplexed magnetic Luminex assay

Tumor samples were processed as described previously.[8 27] Briefly, samples were homogenized and incubated in ice-cold Lysis Buffer #11 (R&D Systems) with protease inhibitors (1 hour, 4°C). The samples were then centrifuged (14 000 rpm, 20 min, 4°C) to collect the supernatants. The cytokine/chemokine profiling was performed by Eve Technologies Corporation (Calgary, AB Canada) using a multiplexed magnetic Luminex assay.

Bulk RNA-seq and bioinformatic analysis

Tumors were individually homogenized in Buffer RLT Plus, and total RNA was extracted using the RNeasy Plus mini kit (Qiagen) per the manufacturer's protocol. RNA integrity was verified using an Agilent Bioanalyzer (Agilent Technologies). The University of Rochester Genomics Research Center (GRC) performed RNA sequencing, preparing complementary DNA libraries with TruSeq RNA Sample Preparation Kit V.2 (Illumina) and sequencing them on an Illumina high-throughput HiSeq 2500 platform. Differential gene expression analysis was conducted using DESeq2 (V.1.28.1) in R (V.4.0.2), with significant thresholds set at an adjusted p value (p adj <0.05) and abs(log2FoldChange) > 0. Enriched pathways and transcription factors were identified using Enrichr.

ScRNA-seq and bioinformatic analysis

As previously described,[29] mouse tumor tissues were dissociated using the Tumor Dissociation Kit (Miltenyi Biotec 130-096-730), following the guidelines outlined in the 10x Genomics protocol (CG00147.Rev B). The resulting single-cell suspension was stained with Ghost Dye Violet 510, and only viable (unstained) cells were selected through sorting. Cells from various samples were multiplexed, captured, and sequenced in accordance with 10x Genomics protocols at the GRC of the University of Rochester Medical Center.

The raw single-cell RNA sequencing (scRNA-seq) data were processed using the CellRanger software (V.6.0.2) from 10x Genomics, which facilitated demultiplexing and

the generation of raw gene expression counts based on the mm10 reference genome. Downstream analysis was conducted in RStudio (V.4.3.2) using Seurat (V.4.3.0), which enabled quality control, filtering, normalization, clustering, and the identification of cluster-specific marker genes. Cells with mitochondrial genome content exceeding 10% were removed, and thresholds of 200–7,000 detected genes per cell were set to exclude low-quality cells and doublets. Data normalization was carried out using the "SCTransform" function, while principal component analysis (PCA) and uniform manifold approximation and projection (UMAP) were applied for dimensionality reduction and clustering through the "RunPCA" and "RunUMAP" functions, respectively. Cluster-specific marker genes were identified using the "FindAllMarkers" function, while differentially expressed genes between treatment groups within selected clusters were determined via the "FindMarkers" function. To visualize gene expression patterns across cell clusters or treatment conditions, functions such as "VlnPlot," "DotPlot," "FeaturePlot," and "RidgePlot" were used. Genes with an adjusted p value<0.05 and a log2 fold change greater than 0.25 or less than −0.25 were analyzed for pathway enrichment using Enrichr. The average expression levels of upregulated and downregulated genes within relevant signaling pathways were further calculated using the "AddModuleScore" function and represented in RidgePlot or VlnPlot across different treatment conditions.

Statistical analysis

All statistical analyses were performed using GraphPad Prism (V.9.3.1). Unless otherwise specified, results are presented as mean±SEM. For growth curve experiments, multiple comparison, one-way analysis of variance (ANOVA) with Bonferroni post hoc adjustments was used. For survival curve multiple comparisons, the log-rank (Mantel-Cox) with Bonferroni adjustment was applied. In studies involving multiple group comparison, one-way ANOVA followed by the Dunnett test was performed. For direct comparison between two groups, paired Student's t-tests were used. Statistical significance was set at p<0.05 or p<0.01, as indicated.

RESULTS

Combined LIF and PD-L1 blockade enhances SBRT efficacy in orthotopic PDAC models

We evaluated whether targeting LIF and PD-L1 could potentiate SBRT in two immunocompetent PDAC orthotopic models: KCKO-Luc (p48-Cre/LSL-KrasG12D mice-derived) and KP2-Luc (p48-Cre/LSL-KrasG12D/p53flox/+ mice-derived).[8] Mice were randomized into eight groups (figure 1A), including various combinations of SBRT (6Gy×4), anti-LIF, and anti-PD-L1. In the KCKO model (figure 1B–D), significant tumor reduction and improved survival occurred in anti-LIF+anti-PD-L1, SBRT+anti-PD-L1, and the triple therapy when compared with the untreated group. Notably, triple therapy showed superior efficacy, doubling survival rates (50% vs 25%) compared with SBRT+anti-PD-L1. In the KP2 model, triple therapy again demonstrated enhanced tumor control and survival versus untreated or SBRT+anti-PD-L1 groups (figure 1E–G). These results established that concurrent LIF/PD-L1 inhibition synergizes with SBRT, yielding significantly improved outcomes in aggressive PDAC models. The consistent superiority of triple therapy across both models highlights its translational potential for pancreatic cancer treatment.

Blockade of PD-L1 or LIF enhances ICD induced by SBRT

Immunogenic cell death (ICD) promotes antitumor immunity through damage-associated molecular patterns (DAMPs) release and immune cell recruitment.[30 31] While we previously established that SBRT induces ICD in PDAC models,[26 27] and that PD-L1 blockade potentiates this effect,[8] we now investigated whether adding LIF inhibition could further enhance ICD. In KP2 tumors harvested 11 days postimplantation (treatment groups as in figure 1A), we assessed cell death (cleaved caspase 3, figure 2A), and DAMP expression (HMGB1, figure 2B; HSP70, figure 2C). Consistent with previous findings,[8 26 27] SBRT alone induced increased ICD, and the addition of LIF or PD-L1 blockade further augmented cell death when combined with SBRT. The triple therapy (SBRT+anti-PD-L1+anti-LIF) showed the highest levels of ICD, significantly greater than SBRT alone (p<0.01), and a trend toward higher ICD compared with SBRT+anti-LIF or SBRT+anti-PD-L1. Additionally, analysis of scRNA-seq data revealed high expression levels of Hsp70 family genes in both the SBRT+anti-PD-L1 and triple therapy groups (online supplemental figure 1), consistent with the increased protein expression observed by immunohistochemistry (figure 2C). Similarly, in the KCKO model (online supplemental figure 2), SBRT alone induced ICD, and the addition of either anti-LIF or anti-PD-L1 further enhanced cell death when combined with SBRT, with trends consistent with those observed in the KP2 model.

Triple therapy modulates the TME toward a more immunostimulatory phenotype

We analyzed therapy-induced changes in the TME by quantifying 30 immunomodulatory cytokines and chemokines (spanning both immunosuppressive and immunostimulatory factors) using Luminex technology[8] at day 14 postimplantation (figure 3A). PCA (figure 3B, online supplemental figure 3) revealed distinct clustering for the triple therapy group (red dots) compared with SBRT+anti-PD-L1 (blue dots) or untreated group (black dots). Further analysis demonstrated that triple therapy significantly increased IL-2 and IL-12p70 levels against untreated tumors, while reducing protumor factors such as IL-6, LIF, IL-10, MIP1α/β, and VEGF (figure 3A–C, online supplemental figure 4). These results suggest that triple therapy significantly remodeled the TME, promoting immunostimulation largely through substantial reduction of immunosuppressive factors.

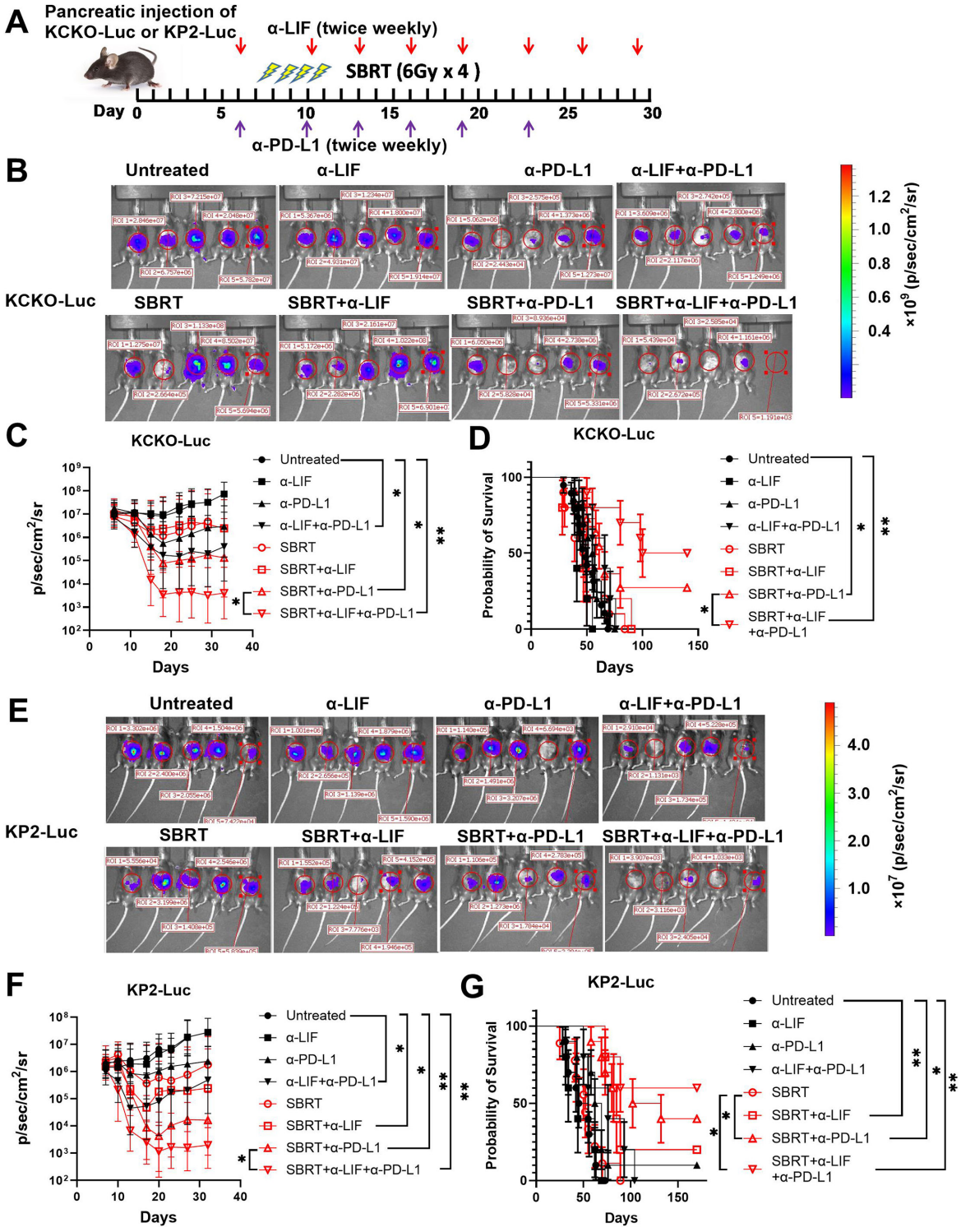

Figure 1 Blockade of LIF and PD-L1 significantly enhances the antitumor efficacy of SBRT in the murine orthotopic model of pancreatic cancer. (A) Schematic of the experimental design. C57BL/6J mice were injected with KCKO-Luc or KP2-Luc cells in the tail of the pancreas and treated with SBRT, anti-LIF, or anti-PD-L1 or combinations of two or three of these. Tumor growth was analyzed by IVIS twice a week. (B) and (E) Representative IVIS images from day 18 after KCKO-Luc (B) or KP2-Luc (E) implantation. (C) and (F) Tumor growth curves in KCKO-Luc (C) or KP2-Luc (F) were determined by IVIS imaging. Data shown are the geometric mean of IVIS value±SD from 10 to 15 mice/group. (D) and (G) Kaplan-Meier survival curves of mice bearing KCKO-Luc (D) or KP2-Luc (G) were observed. For KCKO-Luc model, untreated and SBRT groups (n=15 mice/group), other groups (n=10 mice/group); For KP2-Luc model, untreated (n=15 mice), other groups (n=10 mice/group). *, adjusted p<0.05, **, adjusted p<0.01, analyzed by one-way ANOVA with multiple comparison (adjusted by Bonferroni method) for growth curve; analyzed by log-rank (Mantel-Cox) test with multiple comparison (adjusted by Bonferroni method) for survival curve. ANOVA, analysis of variance; IVIS, in vivo imaging system; KCKO-Luc, luciferase-expressing KCKO; KP2-Luc; luciferase-expressing KP2 cells; LIF, leukemia inhibitory factor; PD-L1, programmed death-ligand 1; SBRT, stereotactic body radiation therapy.

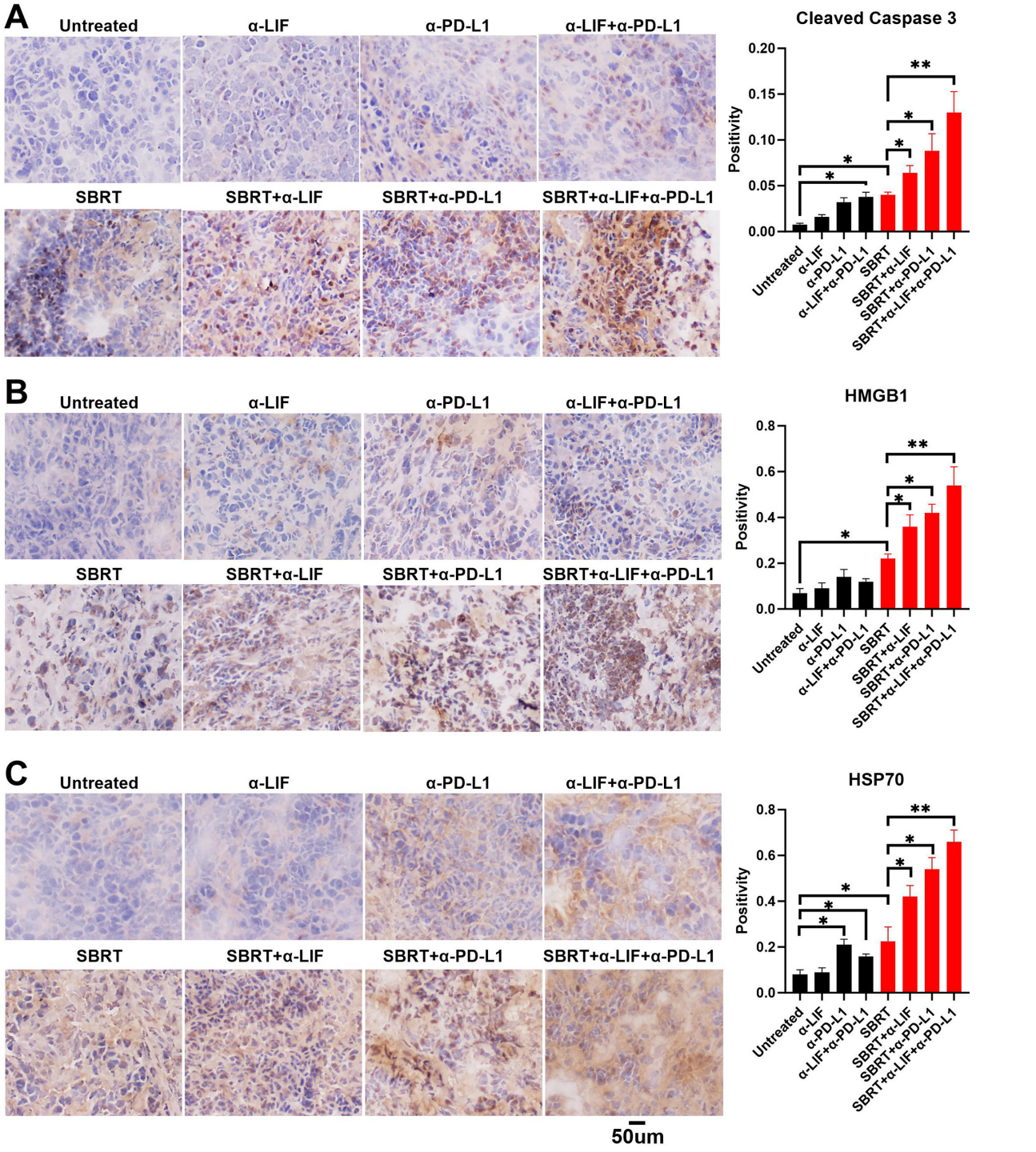

Figure 2 Blockade of PD-L1 or LIF induced increased ICD in combination with SBRT in the orthotopic model of murine pancreatic cancer. Mice bearing KP2-Luc orthotopic tumors were treated with SBRT, anti-LIF or anti-PD-L1, and ICD was determined by immunohistochemistry (IHC) staining of cleaved caspase 3 (A), HMGB1 (B), and HSP70 (C). Results are expressed as the mean positivity±SEM from five mice per group and analyzed by one-way analysis of variance (ANOVA) with Dunnett post-test. *p<0.05, **p<0.01, compared with untreated group or monotherapy group. ICD, immunogenic cell death; KP2-Luc, luciferase-expressing KP2 cells; LIF, leukemia inhibitory factor; PD-L1, programmed death-ligand 1; SBRT, stereotactic body radiation therapy.

Given that macrophages make up the largest proportion of immune cells in the pancreatic TME,[32 33] we evaluated the effect of triple therapy on tumor-infiltrating macrophages using flow cytometry and scRNA-seq. We did not observe significant changes following triple therapy in flow cytometry (online supplemental figures 5 and 6B). However, with scRNA-seq, we revealed distinct phenotypic differences between the macrophages in the triple therapy and SBRT+anti-PD-L1 groups. Specifically, we identified various macrophage subtypes, including

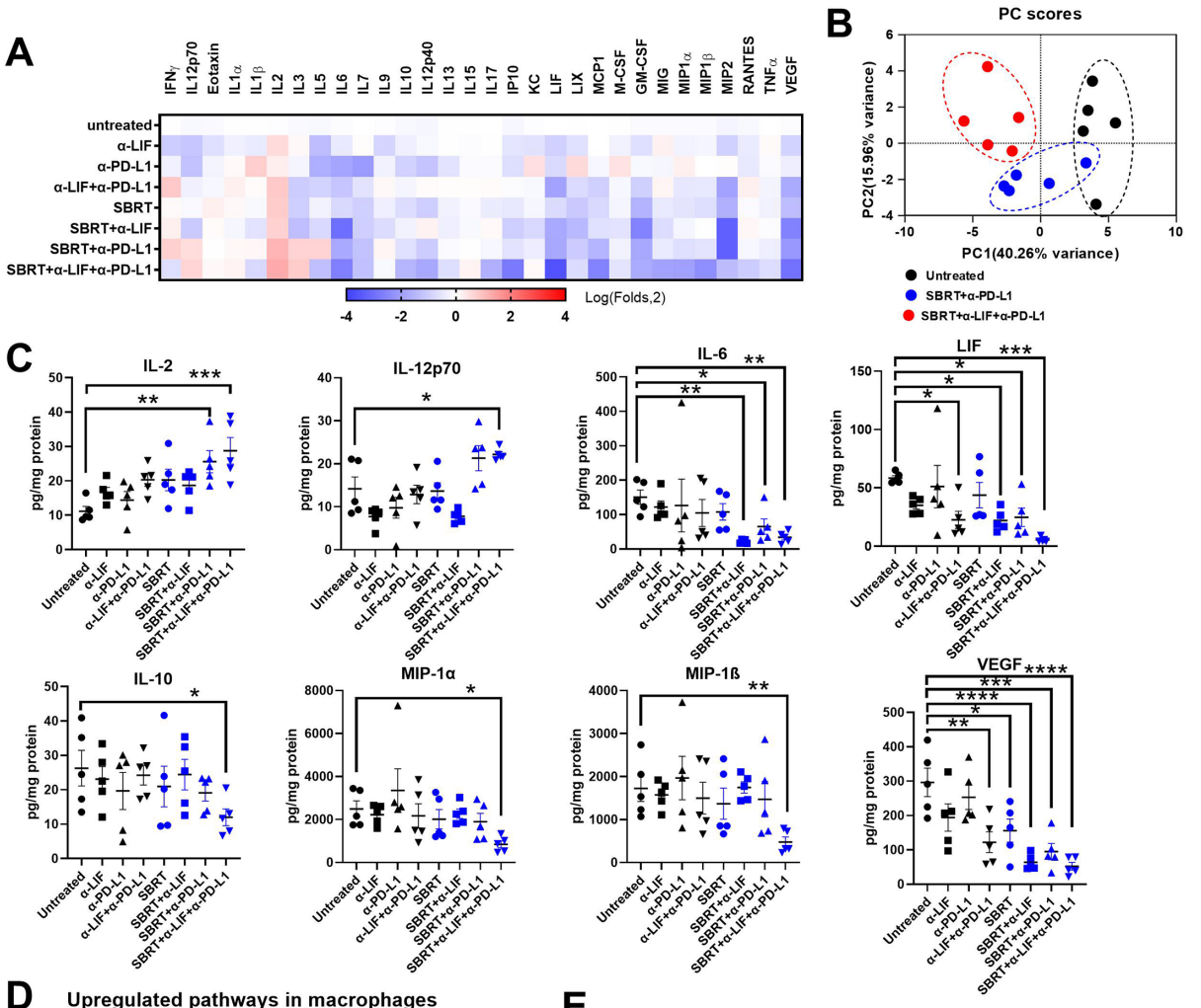

D Upregulated pathways in macrophages (BioPlanet 2019 and MSigDB Hallmark 2020)

Term	p-value
TNF-alpha Signaling via NF-kB	4.736E-37
T cell receptor regulation of apoptosis	2.925E-16
BDNF signaling pathway	1.548E-13
Interleukin-1 regulation of extracellular matrix	2.201E-13
TSH regulation of gene expression	8.833E-13
Toll-like receptor signaling pathway regulation	1.07E-09
Interleukin-5 regulation of apoptosis	1.212E-09
Interleukin-2 signaling pathway	1.778E-09
AP-1 transcription factor network	3.481E-09
Interleukin-1 signaling pathway	8.895E-09

Figure 3 Triple therapy modulates intratumor cytokine/chemokine profiles and macrophage signals toward inflammatory phenotype. The change of intratumoral cytokines and chemokines after therapy was assessed using Luminex technology on day 14 post KCKO-Luc tumor implantation. (A) Fold changes of cytokines and chemokines in the tumor following treatment of SBRT/anti-LIF/anti-PD-L1. The levels of cytokines and chemokines of tumors from no treatment groups were set as 1, and data were fold changes as compared with the untreated group. (B) Principal components analysis (PCA) of cytokine/chemokines comparing untreated, SBRT+anti-PD-L1 and SBRT+anti-LIF+anti-PD-L1 groups. (C) IL-2, IL-12p70, IL-6, LIF, IL-10, MIP-1α, MIP-1β, and VEGF. Results are expressed as mean±SEM from five mice per group and analyzed by one-way ANOVA with Dunnett post-test. Significances are indicated by *p<0.05, **p<0.01, ***p<0.001, and ****p<0.0001 compared with untreated group. (D) and (E) Upregulated pathways in macrophages from scRNA-seq (D) and TNFa, BDNF, TLR and IL2 scores (E) shown in bridge plots. ANOVA, analysis of variance; IFNγ, interferon-gamma; IL, interleukin; KCKO-Luc, luciferase-expressing KCKO; LIF, leukemia inhibitory factor; PD-L1, programmed death-ligand 1; SBRT, stereotactic body radiation therapy; scRNA, single-cell RNA; TLR, Toll-like receptor; TSH, thyroid-stimulating hormone.

monocytes, M1, and M2 macrophages, based on their marker genes (online supplemental figures 7 and 8A–C). Consistent with the previous study that anti-LIF can modulate tumor macrophage activity to enhance the efficacy of antitumor therapy,[24] the triple therapy group exhibited a partial reduction in immunosuppressive M2

macrophages and a significant upregulation of proinflammatory pathways, including TNFα, BDNF, TLR, and IL-2 signaling (figure 3D,E), suggesting enhanced macrophage maturation and activation.[34] Additionally, we observed downregulation of hypoxia, glycolysis, and mTORC1 signals in the triple therapy group compared with the SBRT+anti-PD-L1 group (online supplemental figure 8D,E) further supporting a shift in the TME toward an immunostimulatory phenotype.

CD8+ T cells are critical for triple therapy-induced antitumor efficacy

To assess the effect of SBRT/anti-LIF/anti-PD-L1 on antitumor effector cells, we analyzed tumor-infiltrating immune cell populations via flow cytometry on day 14, 1 day after the third dose of anti-LIF+anti-PD-L1. We observed a notable increase in both $CD8^+$ T cells and $IFN\gamma^+$ $CD8^+$ T cells in the triple therapy group (figure 4A), which the latter was validated using scRNA-seq (online supplemental figure 9). There was no significant change in the percentage of CD4 cells, or myeloid cells within the tumor (online supplemental figure 6).

Using scRNA-seq, we performed a detailed subcluster analysis of $CD8^+$ T cells (online supplemental figure 10A), comparing triple therapy with SBRT+anti-PDL1. Naïve, effector, intermediate cycling (proliferating) and exhausted $CD8^+$ T cell subclusters were identified based on canonical markers (online supplemental figure 10B). Notably, triple therapy exhibited elevated total $CD8^+$ and effector $CD8^+$ cell counts when compared with the SBRT+anti-PD-L1 group (figure 4B,C). Importantly, pathway enrichment analysis revealed significant upregulation of pathways involved in activation of $CD8^+$ T cells,[35] including IL-2 and BDNF (figure 4D,E).

To further evaluate the contribution of $CD8^+$ T cells and $CD4^+$ T cells to the triple therapy-mediated immune response, we performed cell depletion experiments. Depletion of $CD8^+$ T cells led to a significant reduction in the efficacy of triple therapy. Although $CD4^+$ T cell depletion partially diminished the antitumor effect without reaching significance (figure 4F), simultaneous depletion of $CD4^+$ and $CD8^+$ T cells completely eliminated treatment efficacy. These findings underscore the critical role of T cells, particularly $CD8^+$ T cells, in mediating the antitumor effects of the triple therapy. Given that CD8+T cells were identified as critical mediators, we next sought to determine the importance of their production of IFNγ, a potentially key cytokine in the antitumor response. To investigate the critical role of IFNγ in the efficacy of triple therapy, we conducted experiments using IFNγ knockout (IFNγKO) mice. As shown in figure 4G, the antitumor effect of SBRT+anti-LIF+anti-PD-L1 was completely abrogated in IFNγKO mice. Together, these findings highlight the central role of T cells, both as critical effectors and as the primary producers of IFNγ, in mediating the antitumor effects of the triple therapy

Triple therapy leads to a downregulation of stem cell-like transcription and cell growth/metabolism-related pathways, and reduction of EMT

Bulk RNA-seq analysis of whole tumor tissue revealed significant gene expression and pathway changes following treatment. PCA demonstrated distinct separation of the triple therapy group from other treatment groups (figure 5A). Notably, the triple therapy induced downregulation of several key transcription factors associated with tumor stemness, such as MYC, E2F1, SOX2, and RUNX2, as well as pathways related to cell growth, differentiation, and metabolism, including G2-M, EMT, mTORC1, and glycolysis when compared with SBRT+anti-PD-L or untreated groups (figure 5C,D, online supplemental figure 11). Since these transcription factors and pathways are predominately linked to tumor cells, the observed gene expression changes are likely driven by this population. To further investigate this, we conducted scRNA-seq to specifically examine the effects on the tumor cell population.

We performed subclustering of pancreatic tumor cells from the triple therapy and SBRT+anti-PD-L1 groups, which revealed two distinct cell populations of epithelial-like and mesenchymal-like tumor cells based on marker gene expression (online supplemental figure 12A,B). Triple therapy led to an increase in epithelial-like cells and a reduction in mesenchymal-like cells (figure 5E,F). Further pathway enrichment analysis in whole tumor cell population across different treatment groups demonstrated downregulation of Myc and EMT signaling pathways (figure 5G,H), along with upregulation of apoptosis and TNFα signaling pathways (figure 5I,J). These findings align with bulk RNA-seq data (figure 5A–D and online supplemental figure 11) and corroborate previous studies,[14] confirming the role of LIF in regulating tumor cell stemness, EMT and survival.

Triple therapy induces sustained systemic antitumor immune memory

Radiotherapy combined with immunotherapy has been shown to induce systemic or abscopal responses in various tumors, although this effect remains uncertain in PDAC.[36] To evaluate whether triple therapy can induce both local and systemic antitumor responses, we tested mice previously cured of KP2-Luc orthotopic pancreatic tumors using the triple therapy regimen (figure 1). These cured mice were rechallenged with KP2-Luc cells via hemisplenic injection, facilitating liver metastases. As shown in figure 6A,B, naïve mice of comparable age formed liver metastases following the injection. In contrast, mice cured by triple therapy demonstrated complete resistance to metastatic rechallenge, indicating that triple therapy established long-lasting systemic immunity capable of liver tumor rejection. Consistent with this, we noted a significant increase in the activated $CD8^+$ and $CD4^+$ T cells in the spleen of triple therapy-treated mice (figure 6C,D), suggesting the induction of a robust systemic antitumor immune response. Together, these findings indicate that

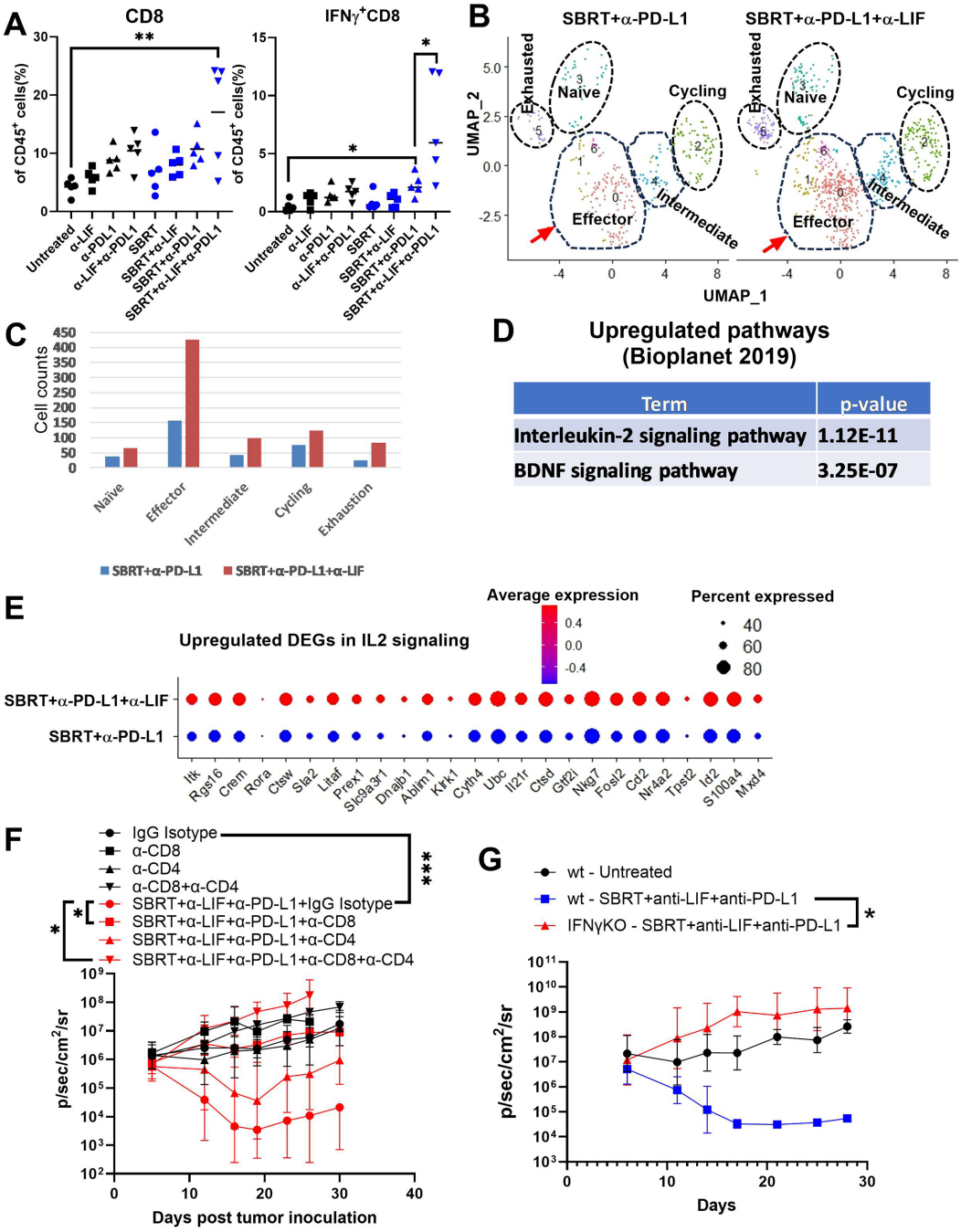

Figure 4 CD8⁺ T cells are critical for the antitumor effect in the orthotopic PDAC model. (A) Mice bearing orthotopic KP2-Luc pancreatic cancer were treated as in figure 1 and sacrificed on day 14. Tumor-infiltrating immune cells were determined by flow cytometry. Tumor-infiltrating CD8⁺ T cells and their expression of IFNγ were analyzed. Results are expressed as mean±SEM from five mice per group and analyzed by ANOVA with Dunnett post-test. Significance is indicated by *p<0.05, **p<0.01. (B–E) Tumor-infiltrating CD8⁺ T cells scRNA-seq analysis. (B) Reclustering of CD8 T cells shown in UMAP. (C) Cell counts in CD8 T cell subtypes across different treatments in pancreatic tumor were depicted, showing that triple therapy induced a relatively high amount of effector CD8 T cells in pancreatic tumor. (D) Upregulated pathways in CD8 T cells (triple therapy vs SBRT+anti-PD-L1 group). (E) DotPlot displaying upregulated DEGs in the IL2 signaling pathway in CD8 T cells from different treatments. (F) Tumor-bearing mice were treated with SBRT+anti-CD73+anti-PD-L1 as in figure 1. Mice were given isotype or antibodies against CD8, CD4 or a combination of both to deplete CD8⁺ T cells, CD4⁺ T cells, or both. Tumor growth was measured by IVIS. Data are represented as geometric mean±SD (n=5 for each group). *p<0.05, ***p<0.001. (G) Wild type or IFNγKO mice bearing KP2-Luc pancreatic cancer were treated as in figure 1. Tumor growth was measured by IVIS. Data are represented as geometric mean±SD (n=5 for each group). *p<0.05. ANOVA, analysis of variance; DEG, differentially expressed genes; IFNγ, interferon-gamma; IL, interleukin; IVIS, in vivo imaging system; KP2-Luc, luciferase-expressing KP2 cells; LIF, leukemia inhibitory factor; PDAC, pancreatic ductal adenocarcinoma; PD-L1, programmed death-ligand 1; SBRT, stereotactic body radiation therapy; scRNA-seq, single-cell RNA sequencing; triple therapy, SBRT+anti-PD-L1+anti LIF; UMAP, uniform manifold approximation and projection.

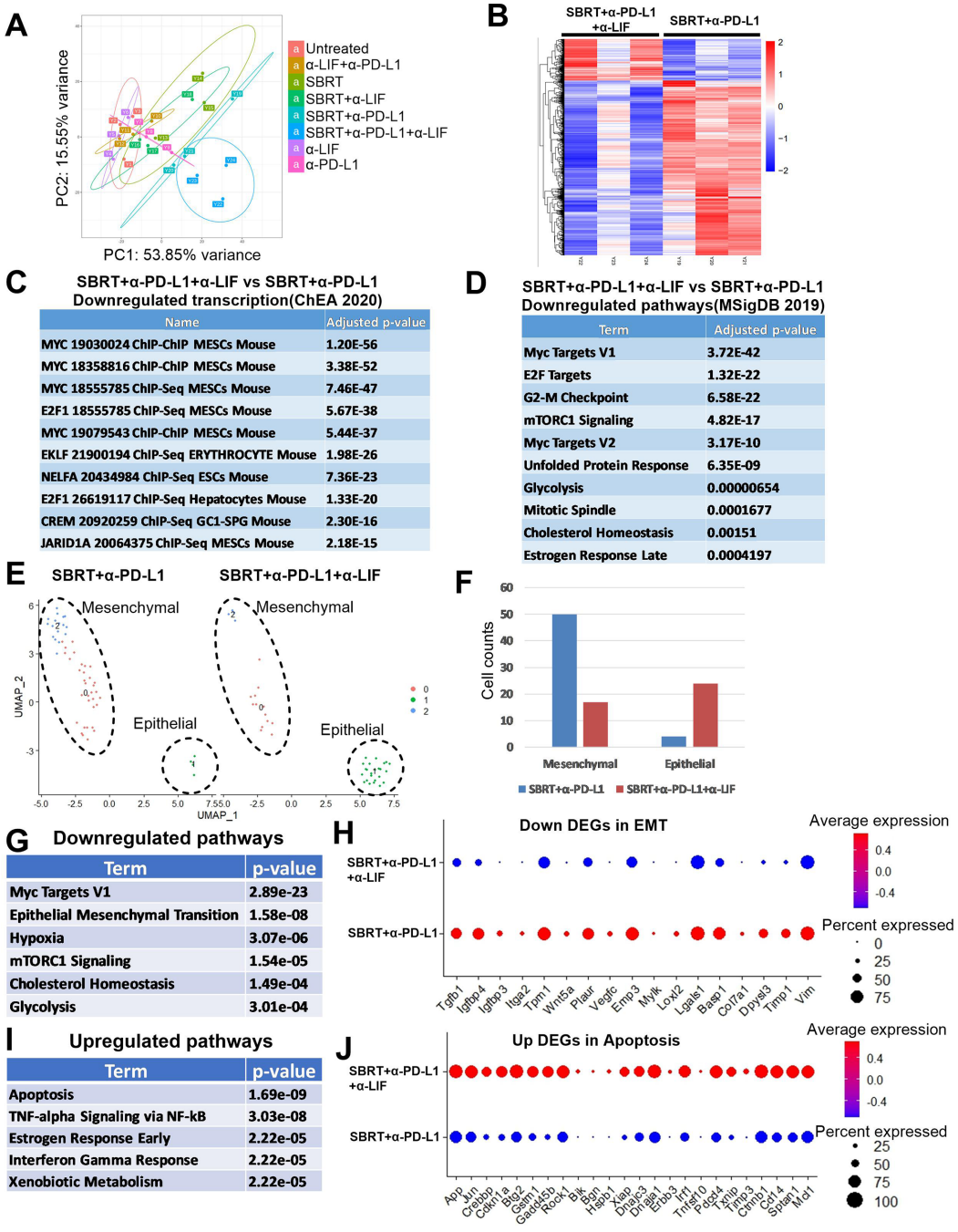

Figure 5 Triple therapy induces downregulation of stem-like transcription, cell cycle-related and metabolism-related pathways and reduction of EMT. (A–D) Mice bearing KCKO-Luc orthotopic pancreatic cancer were treated as in figure 1 and sacrificed on day 14. Tumor tissues were collected and processed for bulk RNA-seq. (A) Principal component analysis was performed showing the samples from triple therapy were relatively separated from other samples from other groups. (B) Heatmap showing the differentially expressed gene in triple therapy versus SBRT+anti-PD-L1 group. (C) Downregulated transcriptions (triple therapy vs SBRT+anti-PD-L1) in tumor stemness. (D) Downregulated pathways (triple therapy vs SBRT+anti-PD-L1) including cell growth (G2-M checkpoint), stemness (Myc, E2F), and metabolism (mTORC1, glycolysis, cholesterol homeostasis). (E–J) Tumor cells scRNA-seq analysis showing that triple therapy induced the reduction of mesenchymal tumor cells. (E) Subclusters of tumor cells across different treatments are shown in UMAP. (F) Cell counts in cell types across different treatments in pancreatic tumors were depicted, showing that triple therapy induced a decrease of mesenchymal cells and an increase of epithelial cells. (G) Downregulated pathways in stemness (Myc, epithelial mesenchymal transition) and metabolisms (Hypoxia, mTORC1, cholesterol homeostasis and glycolysis) when comparing triple therapy versus SBRT+anti-PD-L1. (H) Downregulated DEGs in EMT signal pathway shown in DotPlots. (I) Upregulated pathways when comparing triple therapy versus SBRT+anti-PD-L1. (J) Upregulated DEGs in apoptosis signal pathway shown in DotPlots. DEG, differentially expressed gene; EMT, epithelial to mesenchymal transition; KCKO-Luc, luciferase-expressing KCKO; LIF, leukemia inhibitory factor; PD-L1, programmed death-ligand 1; SBRT, stereotactic body radiation therapy; scRNA-seq, single-cell RNA sequencing; UMAP, uniform manifold approximation and projection.

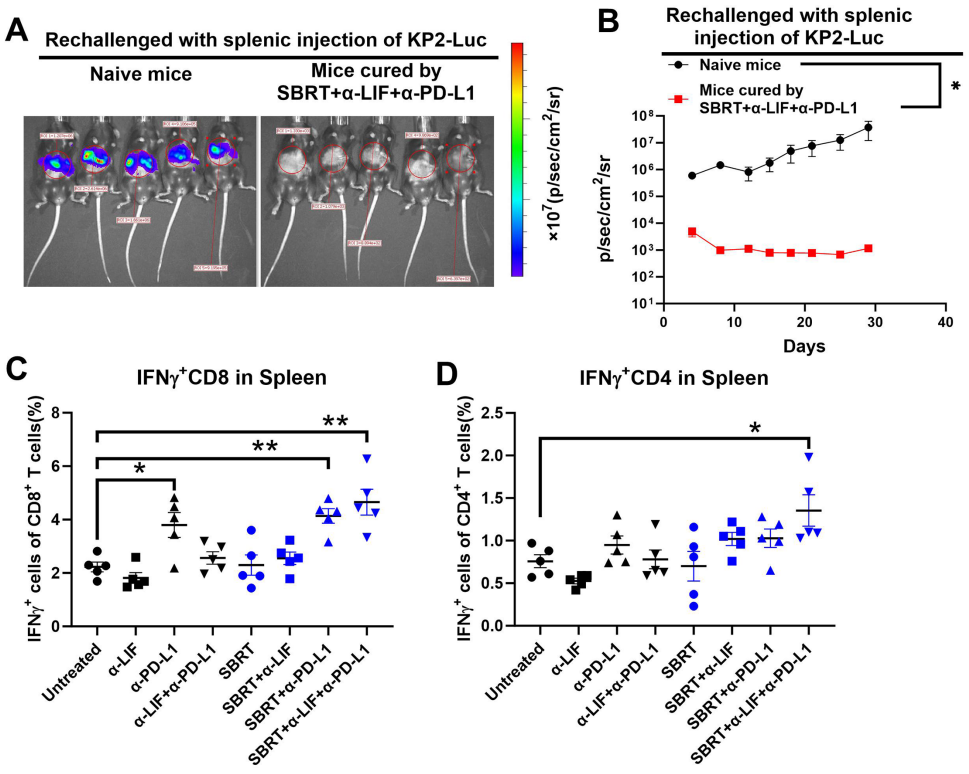

Figure 6 Triple therapy induces systemic antitumor immune response in PDAC model. (A) and (B), mice that were cured by SBRT+anti-LIF+anti-PD-L1 in figure 1 were resistant to tumor rechallenge. Mice cured by triple therapy and age-matched naïve mice received 5×10^5 KP2-Luc cells via hemisplenic injection. Tumor growth was monitored using IVIS imaging. (A) Representative of IVIS on day 7 post injection. (B) Growth curve of tumor liver metastasis (n=5 mice/group). *p<0.05, by multiple t-tests. (C) and (D) Triple therapy with SBRT, anti-PD-L1 and anti-LIF enhances activation of CD8 and CD4 cells in the spleen of murine pancreatic cancer orthotopic models. Mice bearing KP2-Luc orthotopic pancreatic cancer underwent treatment as described in figure 1 and were euthanized on day 14. Immune cells in the spleen were assessed by flow cytometry. Results are presented as mean±SEM from five mice per group and analyzed using ANOVA with Dunnett's post-test. Significance is denoted by *p<0.05. ANOVA, analysis of variance; IFNγ, interferon-gamma; IVIS, in vivo imaging system; KP2-Luc, luciferase-expressing KP2 cells; LIF, leukemia inhibitory factor; PDAC, pancreatic ductal adenocarcinoma; PD-L1, programmed death-ligand 1; SBRT, stereotactic body radiation therapy.

combining systemic LIF/PD-L1 inhibition with localized SBRT generates durable systemic antitumor immunity.

DISCUSSION

LIF has surfaced as a promising therapeutic target in PDAC, as recent preclinical and clinical studies demonstrated that LIF, secreted by pancreatic stellate cells, functions as a pleiotropic regulator in PDAC progression by governing the cancer stem cells self-renewal, cancer-associated fibroblasts activation, suppressive myeloid cells modulation, tumor cell proliferation, and chemoresistance. Phase 1 clinical trials demonstrated tolerability and safety of a humanized monoclonal antibody against LIF, however the efficacy was limited.[25] Therefore, combining LIF blockade with existing treatment modalities (radiotherapy, chemotherapies, and immunotherapies) may overcome the therapeutic resistance of PDAC. In our study, systemic anti-LIF/anti-PD-L1 combined with localized SBRT enhanced tumor control in multiple orthotopic PDAC models. Importantly, this triple therapy also elicited durable systemic antitumor immunity.

Our data suggest that anti-LIF when used in the triple therapy regimen may target multiple cell types within the TME. Bulk RNA-seq analysis identified tumor cells as a primary target, revealing notable downregulation of stemness, EMT, and proliferation-related pathways in response to triple therapy (figure 5A–D and online supplemental figure 11), consistent with prior reports of LIF's role in regulating tumor cell behavior. Additionally, scRNA-seq in the KP2 model further demonstrated a decrease in mesenchymal-like tumor cells and an increase in epithelial-like tumor cells (figure 5E–F and online supplemental figure 12). This was accompanied by the downregulation of Myc and EMT pathways, and the upregulation of apoptosis and the TNFα pathways (figure 5G–J). Addition of anti-LIF treatment to SBRT+anti-PD-L1 also downregulated several metabolic pathways, including mTORC1, glycolysis, and cholesterol homeostasis (figure 5D, online supplemental figure 11C), which have not been widely reported in PDAC. Supporting our findings, a recent study in breast cancer has demonstrated LIF's role in metabolic rewiring specifically by

activating AKT to promote Glut1 trafficking to the plasma membrane, thereby increasing glucose uptake and glycolytic activity to drive tumor progression.[37] Additionally, mutant KRAS has been shown to activate the cholesterol biosynthesis pathway through downstream PI3K/AKT/mTOR signaling, promoting tumor progression in PDAC models.[38] Together, our findings suggest that the addition of anti-LIF may result in further metabolic reprogramming in PDAC tumor cells, including glycolysis and cholesterol homeostasis, which could be critical in mediating the antitumor effects observed with triple therapy.

LIF targeting in cancers, especially PDAC, has primarily focused on tumor cell biology.[13 14 19 39] ICD is a key mechanism for initiating antitumor immune responses, making it an important target for enhancing therapy. In a prior study on nasopharyngeal cancer, LIF was shown to hinder the DNA damage response through activation of m-TORC1/p70S6K signaling, and inhibiting LIF enhanced sensitivity to radiation.[18] However, the role of LIF mediating radioresistance in PDAC has not been explored until now. Our data indicate that, in the KP2 model, the combination of anti-LIF and SBRT increases ICD (figure 2) and is associated with improved antitumor efficacy (figure 1F,G). This is further supported by the downregulation of the mTORC1 pathway following anti-LIF treatment (figure 5G), indicating a potential link between LIF inhibition and augmented DNA damage response. Further studies are required to characterize the precise mechanisms by which LIF may mediate treatment efficacy through ICD induction.

PDAC is characterized by a profoundly immunosuppressive TME that is driven primarily by abundant suppressive myeloid cells. LIF is a cytokine known for its immunosuppressive effects with emerging evidence suggesting blocking LIF may enhance ICB,[16 40] though its immunoregulatory role in PDAC remains largely unexplored. We investigated whether anti-LIF can repolarize the TME toward immunostimulant and enhance antitumor immune responses, particularly when combined with SBRT and immunotherapy. We demonstrated that the triple therapy regimen significantly alters the immune TME as evidenced by several key observations: First, there is a marked change in the cytokine/chemokine profile, with increased levels of IL2 and IL12, and decreased expression of inhibitory factors such as IL6, LIF, IL10, MIP1α, MIP1β, and VEGF (figure 3). Second, we observed a significant increase in $CD8^+$ T cell infiltration, particularly $IFN\gamma^+CD8^+$ cells, within pancreatic tumors (figure 4A). Additionally, scRNA-seq data (figure 4B–E) revealed increased tumor-infiltrating effector $CD8^+$ T cells and upregulated IL2 signaling pathways. Importantly, the antitumor efficacy of the triple therapy is largely dependent on $CD8^+$ T cells, as demonstrated by the loss of efficacy on $CD8^+$ T cell depletion (figure 4F). Finally, anti-LIF also reshapes tumor-infiltrating myeloid cells, including macrophages, promoting an antitumor phenotype (online supplemental figure 8, figure 3D,E). Collectively, these results underscore the promise of anti-LIF therapy when combined with SBRT and immunotherapy to transform the immunosuppressive TME in PDAC, fostering a more immunostimulatory milieu that boosts antitumor immunity.

Anti-LIF treatment has been shown to enhance the tumor immune response by shifting tumor-associated macrophage (TAM) polarization from M2 to M1 phenotype and increasing CXCL9 expression, consequently promoting the infiltration of effector $CD8^+$ T cells into the TME.[16] Although our study did not detect significant changes in CXCL9 levels following treatment, we observed a significant decrease in several inhibitory factors within the TME, including macrophage-derived MIP-1α and MIP-1β (figure 3, online supplemental figure 4). Furthermore, we identified upregulated proinflammatory signaling pathways, such as TNFα, BDNF, TLR, and IL2 in macrophages (figure 3D,E). It has been reported that PDAC cells induce metabolic reprogramming in macrophages, shifting their energy production from oxidative phosphorylation to glycolysis. This metabolic switch drives macrophage polarization towards an M2 phenotype, which facilitates tumor progression and invasion.[32 41 42] The observed reduction in M2 macrophages following triple therapy may result from the suppression of metabolic pathways, including glycolysis in these immune cells (online supplemental figure 8C,E). Taken together, these results suggest that anti-LIF therapy reprograms TAMs towards an antitumor state in PDAC models.

Collectively, the triple therapy exerts dual effects by directly targeting tumor cells and broadly reshaping the antitumor immune response. Our findings reveal a distinct anti-LIF treatment signature characterized by decreased tumor stemness, proliferation, and metabolic signaling, accompanied by heightened infiltration of effector $CD8^+$ T cells and enhanced macrophage activation/maturation. Additionally, we demonstrate that SBRT combined with LIF and PD-L1 blockade generates not only localized but also sustained systemic antitumor immunity in PDAC (figure 6). In conclusion, our findings suggest that the triple therapy regimen involving SBRT, anti-LIF, and anti-PD-L1 holds promise for overcoming immunosuppressive barriers in PDAC both locally and systemically. Ongoing clinical trials evaluating combined ICB, anti-LIF, and chemotherapy in PDAC (NCT04999969) represent a critical step toward clinical translation of our triple therapy approach. These results provide preclinical validation for a triple therapy approach combining SBRT, anti-LIF, and anti-PD-L1 as a neoadjuvant or adjuvant treatment strategy in human PDAC.

Author affiliations
[1]Department of Surgery, University of Rochester Medical Center, Rochester, New York, USA
[2]Center for Tumor Immunology Research, University of Rochester Medical Center, Rochester, New York, USA
[3]Department of Microbiology and Immunology, University of Rochester Medical Center, Rochester, New York, USA
[4]Genomic Research Center, University of Rochester Medical Center, Rochester, New York, USA

[5]Wilmot Cancer Institute, University of Rochester Medical Center, Rochester, New York, USA
[6]Department of Pediatrics, University of Rochester Medical Center, Rochester, New York, USA
[7]Department of Medicine Hematology/Oncology, University of Rochester Medical Center, Rochester, New York, USA
[8]The Discovery Center, Cambridge Biomedical Campus, Cambridge, UK
[9]Oncology R&D, Research and Early Development, AstraZeneca R&D, Cambridge, UK

X Gary Hannon @GaryHannon10

Acknowledgements We thank Eric Hernady and Brian Marples from Wilmot Cancer Center Imaging and Radiation Shared Resource for mice SBRT treatment.

Contributors Conception and design: JY and SAG. Development of methodology: JY, CJJ, RJ, SL and SAG. Acquisition of data: JY, ALH, GH, TGV, and MLL. Analysis and interpretation of data: JY, SSQ, LB, NAS, LMC and SAG. Writing, review, and/or revision of the manuscript: JY, EL, GH, SLE, NL, JE and SAG. Administrative, technical, or material support: ALH, BNM, CJJ, BAB and JE. Guarantors: JY and SAG. Study supervision: DL and SAG.

Funding This research was supported by AstraZeneca and funding from the National Institutes of Health (R01CA230277 to SAG; R01CA236390 to SAG; R01CA262580 to SAG, T32AI007285 to TGV, and DL; R01CA168863 to DL).

Competing interests JE and NL hold AstraZeneca stock.

Patient consent for publication Not applicable.

Ethics approval University Committee on Animal Resources (UCAR) in University of Rochester. UCAR number: UCAR-2014-037E.

Provenance and peer review Not commissioned; externally peer reviewed.

Data availability statement All data relevant to the study are included in the article or uploaded as supplementary information.

ORCID iDs
Jian Ye http://orcid.org/0000-0002-6955-9262
Gary Hannon http://orcid.org/0000-0003-1204-0299

REFERENCES

1 Rahib L, Smith BD, Aizenberg R, *et al*. Projecting cancer incidence and deaths to 2030: the unexpected burden of thyroid, liver, and pancreas cancers in the United States. *Cancer Res* 2014;74:2913–21.
2 Siegel RL, Miller KD, Wagle NS, *et al*. Cancer statistics, 2023. *CA Cancer J Clin* 2023;73:17–48.
3 Doroshow DB, Bhalla S, Beasley MB, *et al*. PD-L1 as a biomarker of response to immune-checkpoint inhibitors. *Nat Rev Clin Oncol* 2021;18:345–62.
4 Haslam A, Gill J, Prasad V. Estimation of the Percentage of US Patients With Cancer Who Are Eligible for Immune Checkpoint Inhibitor Drugs. *JAMA Netw Open* 2020;3:e200423.
5 O'Reilly EM, Oh D-Y, Dhani N, *et al*. Durvalumab With or Without Tremelimumab for Patients With Metastatic Pancreatic Ductal Adenocarcinoma: A Phase 2 Randomized Clinical Trial. *JAMA Oncol* 2019;5:1431–8.
6 Royal RE, Levy C, Turner K, *et al*. Phase 2 trial of single agent Ipilimumab (anti-CTLA-4) for locally advanced or metastatic pancreatic adenocarcinoma. *J Immunother* 2010;33:828–33.
7 Zhao P, Li L, Jiang X, *et al*. Mismatch repair deficiency/microsatellite instability-high as a predictor for anti-PD-1/PD-L1 immunotherapy efficacy. *J Hematol Oncol* 2019;12:54.
8 Ye J, Gavras NW, Keeley DC, *et al*. CD73 and PD-L1 dual blockade amplifies antitumor efficacy of SBRT in murine PDAC models. *J Immunother Cancer* 2023;11:e006842.
9 Rech AJ, Dada H, Kotzin JJ, *et al*. Radiotherapy and CD40 Activation Separately Augment Immunity to Checkpoint Blockade in Cancer. *Cancer Res* 2018;78:4282–91.
10 Nicola NA, Babon JJ. Leukemia inhibitory factor (LIF). *Cytokine Growth Factor Rev* 2015;26:533–44.
11 Wang J, Chang CY, Yang X, *et al*. Leukemia inhibitory factor, a double-edged sword with therapeutic implications in human diseases. *Mol Ther* 2023;31:331–43.
12 Peñuelas S, Anido J, Prieto-Sánchez RM, *et al*. TGF-beta increases glioma-initiating cell self-renewal through the induction of LIF in human glioblastoma. *Cancer Cell* 2009;15:315–27.
13 Wang MT, Fer N, Galeas J, *et al*. Blockade of leukemia inhibitory factor as a therapeutic approach to KRAS driven pancreatic cancer. *Nat Commun* 2019;10:3055.
14 Shi Y, Gao W, Lytle NK, *et al*. Targeting LIF-mediated paracrine interaction for pancreatic cancer therapy and monitoring. *Nature New Biol* 2019;569:131–5.
15 Albrengues J, Bourget I, Pons C, *et al*. LIF mediates proinvasive activation of stromal fibroblasts in cancer. *Cell Rep* 2014;7:1664–78.
16 Pascual-García M, Bonfill-Teixidor E, Planas-Rigol E, *et al*. LIF regulates CXCL9 in tumor-associated macrophages and prevents $CD8^+$ T cell tumor-infiltration impairing anti-PD1 therapy. *Nat Commun* 2019;10:2416.
17 McLean K, Tan L, Bolland DE, *et al*. Leukemia inhibitory factor functions in parallel with interleukin-6 to promote ovarian cancer growth. *Oncogene* 2019;38:1576–84.
18 Liu S-C, Tsang N-M, Chiang W-C, *et al*. Leukemia inhibitory factor promotes nasopharyngeal carcinoma progression and radioresistance. *J Clin Invest* 2013;123:5269–83.
19 Bressy C, Lac S, Nigri J, *et al*. LIF Drives Neural Remodeling in Pancreatic Cancer and Offers a New Candidate Biomarker. *Cancer Res* 2018;78:909–21.
20 Kellokumpu-Lehtinen P, Talpaz M, Harris D, *et al*. Leukemia-inhibitory factor stimulates breast, kidney and prostate cancer cell proliferation by paracrine and autocrine pathways. *Int J Cancer* 1996;66:515–9.
21 Ohata Y, Tsuchiya M, Hirai H, *et al*. Leukemia inhibitory factor produced by fibroblasts within tumor stroma participates in invasion of oral squamous cell carcinoma. *PLoS One* 2018;13:e0191865.
22 Viswanadhapalli S, Luo Y, Sareddy GR, *et al*. EC359: A First-in-Class Small-Molecule Inhibitor for Targeting Oncogenic LIFR Signaling in Triple-Negative Breast Cancer. *Mol Cancer Ther* 2019;18:1341–54.
23 Yue X, Wu F, Wang J, *et al*. EC330, a small-molecule compound, is a potential novel inhibitor of LIF signaling. *J Mol Cell Biol* 2020;12:477–80.
24 Hallett RM, Bonfill-Teixidor E, Iurlaro R, *et al*. Therapeutic Targeting of LIF Overcomes Macrophage-mediated Immunosuppression of the Local Tumor Microenvironment. *Clin Cancer Res* 2023;29:791–804.
25 Borazanci E, Schram AM, Garralda E, *et al*. Phase I, first-in-human study of MSC-1 (AZD0171), a humanized anti-leukemia inhibitory factor monoclonal antibody, for advanced solid tumors. *ESMO Open* 2022;7:100530.
26 Ye J, Mills BN, Zhao T, *et al*. Assessing the Magnitude of Immunogenic Cell Death Following Chemotherapy and Irradiation Reveals a New Strategy to Treat Pancreatic Cancer. *Cancer Immunol Res* 2020;8:94–107.
27 Ye J, Mills BN, Qin SS, *et al*. Toll-like receptor 7/8 agonist R848 alters the immune tumor microenvironment and enhances SBRT-induced antitumor efficacy in murine models of pancreatic cancer. *J Immunother Cancer* 2022;10:e004784.
28 Mills BN, Connolly KA, Ye J, *et al*. Stereotactic Body Radiation and Interleukin-12 Combination Therapy Eradicates Pancreatic Tumors by Repolarizing the Immune Microenvironment. *Cell Rep* 2019;29:406–21.
29 Ye J, Qin SS, Hughson AL, *et al*. Blockade of LIF and PD-L1 Enhances Chemotherapy in Preclinical PDAC Models. *Cancers (Basel)* 2025;17:204.
30 Galluzzi L, Guilbaud E, Schmidt D, *et al*. Targeting immunogenic cell stress and death for cancer therapy. *Nat Rev Drug Discov* 2024;23:445–60.
31 Arimoto KI, Miyauchi S, Liu M, *et al*. Emerging role of immunogenic cell death in cancer immunotherapy. *Front Immunol* 2024;15:1390263.

32 Bandi DSR, Sarvesh S, Farran B, *et al*. Targeting the metabolism and immune system in pancreatic ductal adenocarcinoma: Insights and future directions. *Cytokine Growth Factor Rev* 2023;71–72:26–39.
33 Poh AR, Ernst M. Tumor-Associated Macrophages in Pancreatic Ductal Adenocarcinoma: Therapeutic Opportunities and Clinical Challenges. *Cancers (Basel)* 2021;13:2860.
34 Asami T, Ito T, Fukumitsu H, *et al*. Autocrine activation of cultured macrophages by brain-derived neurotrophic factor. *Biochem Biophys Res Commun* 2006;344:941–7.
35 Xiao R, Bergin SM, Huang W, *et al*. Environmental and Genetic Activation of Hypothalamic BDNF Modulates T-cell Immunity to Exert an Anticancer Phenotype. *Cancer Immunol Res* 2016;4:488–97.
36 Xing D, Siva S, Hanna GG. The Abscopal Effect of Stereotactic Radiotherapy and Immunotherapy: Fool's Gold or El Dorado? *Clin Oncol (R Coll Radiol)* 2019;31:432–43.
37 Yue X, Wang J, Chang C-Y, *et al*. Leukemia inhibitory factor drives glucose metabolic reprogramming to promote breast tumorigenesis. *Cell Death Dis* 2022;13:370.
38 Duan X, Zhang T, Feng L, *et al*. A pancreatic cancer organoid platform identifies an inhibitor specific to mutant KRAS. *Cell Stem Cell* 2024;31:71–88.
39 Wrona E, Potemski P, Sclafani F, *et al*. Leukemia Inhibitory Factor: A Potential Biomarker and Therapeutic Target in Pancreatic Cancer. *Arch Immunol Ther Exp (Warsz)* 2021;69:2.
40 Loriot Y, Marabelle A, Guégan JP, *et al*. Plasma proteomics identifies leukemia inhibitory factor (LIF) as a novel predictive biomarker of immune-checkpoint blockade resistance. *Ann Oncol* 2021;32:1381–90.
41 Khalaf K, Hana D, Chou JT-T, *et al*. Aspects of the Tumor Microenvironment Involved in Immune Resistance and Drug Resistance. *Front Immunol* 2021;12:656364.
42 Penny HL, Sieow JL, Gun SY, *et al*. Targeting Glycolysis in Macrophages Confers Protection Against Pancreatic Ductal Adenocarcinoma. *Int J Mol Sci* 2021;22:6350.